A Light-Switchable Exchange-Coupled Magnet

Divya Rajan,[†] John M. Cain,[†] Tatiana Brinzari,[†] Caue F. Ferreira,[†] Nicholas G. Rudawski,[‡] Ashley C. Felts,[†] Mark W. Meisel,[‡] Daniel R. Talham[†]

[†]Department of Chemistry, University of Florida, Gainesville, FL 32611-7200, USA

'Department of Physics and National High Magnetic Field Laboratory, University of Florida, Gainesville, FL 32611-8440, USA

[†] Herbert Wertheim College of Engineering, University of Florida, Gainesville, FL-32611, USA

KEYWORDS: Ferrite magnets; exchange coupling; cobalt ferrite; manganese ferrite; nanomagnets; light-induced magnetization.

ABSTRACT: A light-switchable hard magnet/soft magnet composite is described for which light irradiation breaks the exchange coupling between the two components. Heterostructure composites composed of nanometer scale particles of the hard magnet cobalt ferrite with the soft magnet manganese ferrite show a coherent response in magnetization vs applied field measurements, consistent with exchange coupling, which is disrupted upon illumination causing an inflection at low fields corresponding to the soft magnet manganese ferrite. The light-induced decoupling of the exchange coupled magnets can be attributed to the selective demagnetization at the surface of the ferrite nanoparticles, breaking the interferrite coupling.

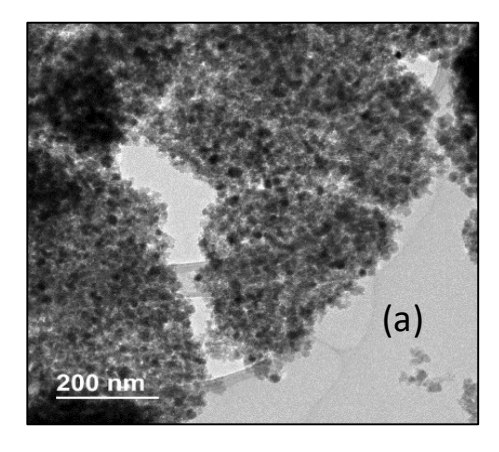
Larger magnetic data storage densities require smaller bit sizes, but even as smaller objects are realized, areal densities become limited by the ability to focus the magnetic write head. To overcome the limitations of write-head focusing, heat-assisted magnetic recording (HAMR) 1-3 was developed whereby a laser is used to locally heat the recording media and lower its energy product to enable recording on strongly anisotropic media. Manipulation of magnetization solely with light, or all-optical switching (AOS), has also been demonstrated for a growing list of potential recording media.4 In AOS, femtosecond laser pulses heat the magnetic system to near the Curie temperature leading to magnetization switching dictated either by the choice of circular polarization or by magnetic sublattice structure.4 With these methods, magnetic information size becomes determined by standards of technologies such as plasmonic focusing or near-field optics, rather than by the ability to focus a magnetic field. However, a potential limitation of these technologies is thermal heating and cycling, which can cause component degradation.2

These drawbacks could be overcome if the energy product of a magnet can be lowered without the need for bulk heating. In this work, a light-switchable hard/soft exchange-coupled magnet is described, demonstrating a new concept with potential application in energy-assisted magnetic recording or switchable microwave absorption. Exchange-coupled magnets are nanocomposites with potential applications in diverse fields spanning from energy to biomedicine.⁵⁻⁹ Exchange-coupling between a ferromagnet and antiferromagnet generates an extra source of anisotropy due to the component interface and a consequent increase in the thermal stability of the magnetization.^{10,11} In

another variation, when a hard permanent magnet is exchange coupled with a soft magnet having higher magnetization, the energy product of the composite is enhanced. The soft phase becomes enslaved to the hard phase and the composite responds coherently to temperature and applied magnetic field.^{6,12,7,13} Studies have shown exchange-coupled magnets represent an effective approach to tackling the competing technical demands associated with miniaturizing magnets while at the same time maintaining viable properties, such as thermal stability of magnetization and coercivity, both of which decrease as magnetic particles approach the superparamagnetic limit.^{3,8,10}

The concept for a light-switchable exchange coupled magnet derives from the fact that exchange coupling depends on interactions between moments at the interface between the two coupled materials.⁶ If exchange at the interface is broken, the soft component reverts and the energy product of a hard magnet/soft magnet composite decreases. Therefore, a light-based process to selectively alter the interface coupling would eliminate the need for thermal heating of the bulk material. The recent observation of light-induced demagnetization in some cobalt ferrite and manganese ferrite nanoparticles provides an opportunity to demonstrate the concept. Cobalt ferrite nanoparticles were shown by Giri et al.14,15 to undergo lightactivated decrease in coercivity. A more recent study revealed white light irradiation also decreases high field magnetization.¹⁶ The light-induced demagnetization effects were attributed to decoupling of the surface spins leading to a change in volume of the magnetically ordered domains. The broken symmetry and reduced numbers of exchange pathways mean the surface spins decouple on a

different energy scale than the bulk.^{17,18,19-22} A key observation was larger effects are seen for aggregates of particles relative to isolated nanoparticles, indicating the light process also reduces interparticle coupling.¹⁶ If the same processes are applied to a composite material pairing a hard magnet with a soft magnet, a light-switchable exchange coupled magnet should result, providing a mechanism to amplify the effect of the light.



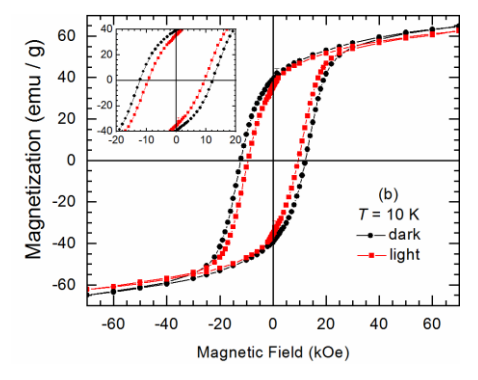


Figure 1. (a) TEM micrographs of $Co_{0.94}Fe_{2.06}O_4$, 1. The particle size distribution within larger aggregates is 12 \pm 4 nm (see supporting information for histogram). (b) Magnetization vs field hysteresis for 1 in the dark and light states at 10 K with an expanded view as an inset.

Examples of cobalt ferrite-based exchange-coupled magnets are known with core-shell heterostructures, for exam-FePt@CoFe₂O₄,²³ $ZnFe_2O_4@CoFe_2O_4^{24}$ MnFe₂O₄@CoFe₂O₄⁸. In this study, manganese ferrite was chosen as the soft magnet to couple with cobalt ferrite, building on our earlier work.¹⁶ Good epitaxy is expected as the two ferrite materials have a relatively small lattice mismatch of around 1.7 %.25 Using surfactant-free coprecipitation methods, cobalt ferrite, 1, and two cobalt ferrite/manganese ferrite particle composites, 2 and 3, were prepared, as described in detail in Supporting Information. The cobalt ferrite (**Figure 1**), with average size of 12 ± 4 nm within aggregates of average size 250 ± 70 nm, analyzed for Co_{0.94}Fe_{2.06}O₄ by ICP. These cobalt ferrite particles were used as seeds to generate a core-shell-like heterostructure of cobalt ferrite@manganese ferrite, 2, following addition of the shell material precursors to a suspension of the seed particles. The resulting aggregates (Figure 2) have a size of 270 ± 80 nm and are composed of nanoparticles with average size 16 ± 4 nm. The ICP-AES analyses indicate the two ferrites are present in a 1:1 ratio, consistent with precursor amounts used in the synthesis. The small difference in the electron density of the two materials means there is no contrast between the two components in TEM micrographs, although energy dispersive X-ray spectroscopy line scans (Figure 2) reveal the elements Co, Mn and Fe are uniformly detected across the particle aggregates, indicating the Mn_{0.94}Fe_{2.06}O₄ precipitates over the preformed $Co_{0.04}Fe_{2.06}O_4$ seeds. In contrast to 2, which may be thought of as a core-shell-like heterostructure, 3 is a more intimate mixture, prepared by simultaneous precipitation of the two ferrites. For 3, the aggregates average 250 ± 70 nm and the nanoparticles within the aggregates are somewhat smaller, with average diameter of 4 ± 1 nm, Figure 3. The 2:1 cobalt:manganese ratio used in the synthesis is reflected in the 2:1 cobalt ferrite:manganese ferrite ratio determined by ICP-AES analyses of the products. Although the separate ferrites cannot be discerned in the electron microscopy and some degree of ion mixing cannot be ruled out, observation of the two components in magnetic measurements and fitting of the powder XRD pattern (supporting information) confirm 3 is best described as a heterostructure composite rather than a solid-solution.

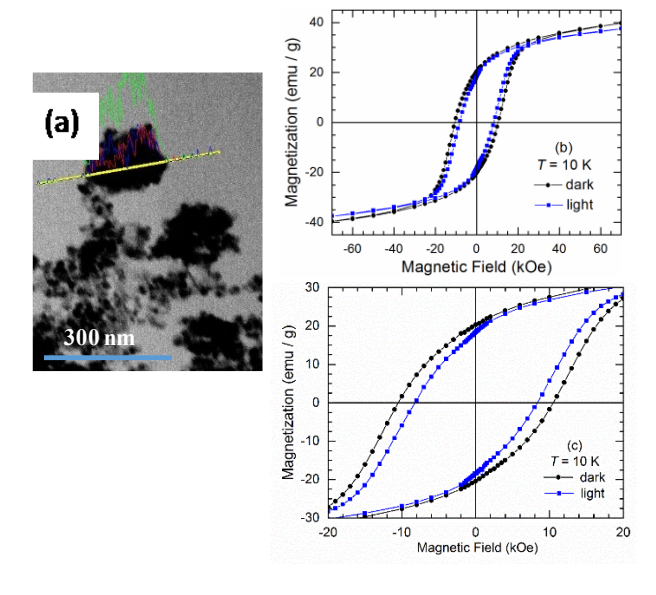
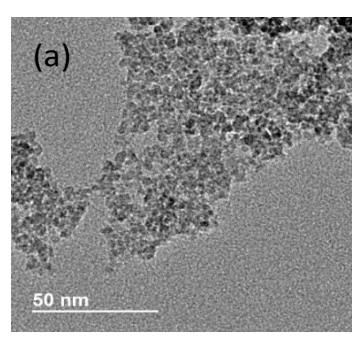


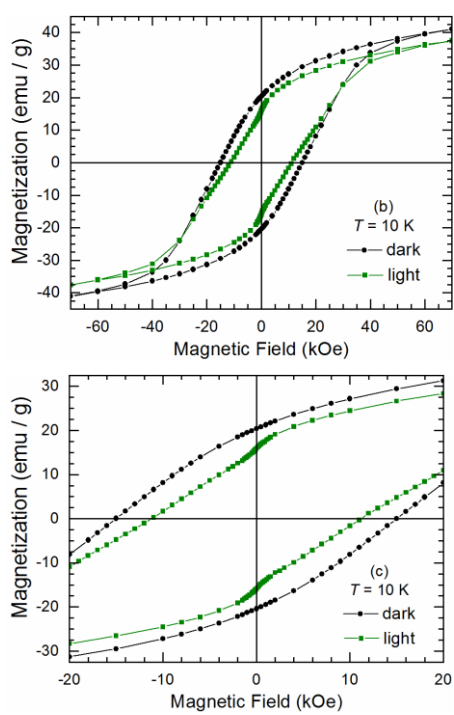
Figure 2. TEM image and magnetometry data for 2. (a) TEM micrograph showing the aggregate on which the electron beam was scanned to obtain corresponding EDS line scans (particle size histogram and complete EDS scans appear in supporting information, Figure S2). (b) Magnetization vs field hysteresis for 2 in the dark and light states at 10 K swept +/- 70 kOe. (c) Expanded view of the +/- 20 kOe region from (b).

Magnetization vs field plots for 1 at 10 K are shown in **Figure 1** with and without white light irradiation. The dark state coercivity of 12.17 \pm 0.04 kOe decreases to 9.43 \pm 0.09 kOe with light and is accompanied by a reduction in the remnant and high field magnetization values. This be-

havior with light is consistent with earlier reports¹⁴⁻¹⁶ on cobalt ferrite nanoparticles and has been attributed to decoupling of surface spins on the nanoparticles resulting in a reduction of magnetic volume and changing interparticle interactions within the aggregates.¹⁶ Similar magnetization vs field plots with and without light for the core-shell-like 2 are presented in Figure 2. The hysteresis loop in the absence of light indicates a coherent response of the two components to the applied magnetic field, consistent with an exchange-coupled system. The lack of contrast between the core and shell material in the TEM analyses does not clearly discern the shell component, however the magnetization vs field response provides an upper limit to the thickness of the manganese ferrite shell. For an exchangecoupled system to coherently respond to temperature and field, the thickness of the soft phase should be less than twice the domain wall width of the hard magnet. 23,26,13 The domain wall width of cobalt ferrite has been calculated to be 8 nm indicating the manganese ferrite should be no thicker than 16 nm to give a coherent response.8 The change in particle size upon precipitating the manganese ferrite is less than 16 nm, which is within the expected requirements for an exchange coupled heterostructure. Just as for cobalt ferrite, the coercivity of 2 decreases with light. The dark state coercivity of 10.50 \pm 0.01 kOe decreases to 8.28 ± 0.08 kOe, with a change of $\Delta H_c = 2.74 \pm 0.10$ kOe, which is comparable with the change seen for 1. However, in contrast to 1, there is a small inflexion in the light state plot for 2 near 1 kOe. Although the magnitude of the change is small, this low-field feature in the hysteresis loop indicates magnetic decoupling.

Exchange coupling in nanocomposite heterostructures depends critically on component dimensions and interface coupling,27 and one-pot syntheses to increase contact between components has often resulted in better magnetic response.²⁸⁻³⁰ This approach was used for the synthesis of 3, in which the hard and soft ferrites were coprecipitated forming an intimate mixture of the two compounds. While magnetometry and PXRD confirm two components, TEM, EDS and EELS analyses could not discern the separate ferrites, so individual compositional domains are no larger than a few nm. As for 2, magnetization vs. field plots for 3 show a coherent magnetic response with a coercivity of 15.01 ± 0.01 kOe at 10 K, Figure 3, again indicating an exchange-coupled mixture of cobalt ferrite-manganese ferrite. While the value of the coercive field for 2 was smaller than for the pure cobalt ferrite, 1, the coercive field for 3, is larger. The behavior parallels observations by Song et al.8 for exchanged coupled CoFe₂O₄@MnFe₂O₄ nanoparticles prepared by thermal decomposition techniques, where the coercive field first increased upon addition of a thin, ~1 nm, manganese ferrite shell but then decreased for successively thicker shells. Once again, upon irradiating with white light the coercivity decreases, Figure 3. For 3, the change, ΔH_c = 3.80 ± 0.01 kOe, is even larger than seen for the pure phase cobalt ferrite. However, the most striking feature is a significant inflection in the light state at low field resulting from magnetic decoupling of the cobalt ferrite and manganese ferrite with light.





Magnetization vs. field of 3 was measured at different temperatures in the dark to confirm the presence of ex

Figure 3. TEM image and magnetometry data for 3. (a) TEM micrograph (Particle size histogram and EELS analysis appear in supporting information, Figure S₃). (b) Magnetization vs field hysteresis for 3 in the dark and light states at 10 K swept \pm 70 kOe. (c) Expanded view of the \pm 70 kOe region of (b).

change-coupled ferrites and explore the thermal requirements needed to break the exchange-coupling. At 10 K the system is exchange-coupled, but with increasing temperature an inflection appears at low field, corresponding to the soft magnet, **Figure 4**. The system is effectively decoupled by 50 K, which is expected to be above the blocking temperature of manganese ferrite nanoparticles.⁸ Based on work on other materials using the same light source and temperature control, we estimate the temperature change of the sample caused by the light source is \leq 0.5 K for temperatures below 50 K. Nevertheless, to verify the observed light-induced behavior is not caused by bulk heating of the

sample, the light-activated changes in the coercivity, remnant and high field magnetization, and magnetization at 70 kOe of 3 were compared to the dark state values at different temperatures in **Figure 4**. The light state values of the coercivity and remnant magnetization at 10 K were comparable to their respective dark state values at ~25-30 K, corresponding to a temperature jump well outside experimental control. Furthermore, high field magnetization in the light state at 10 K is significantly smaller than the high-field value, even at 50 K, providing further evidence the light-state response is not a result of bulk heating.

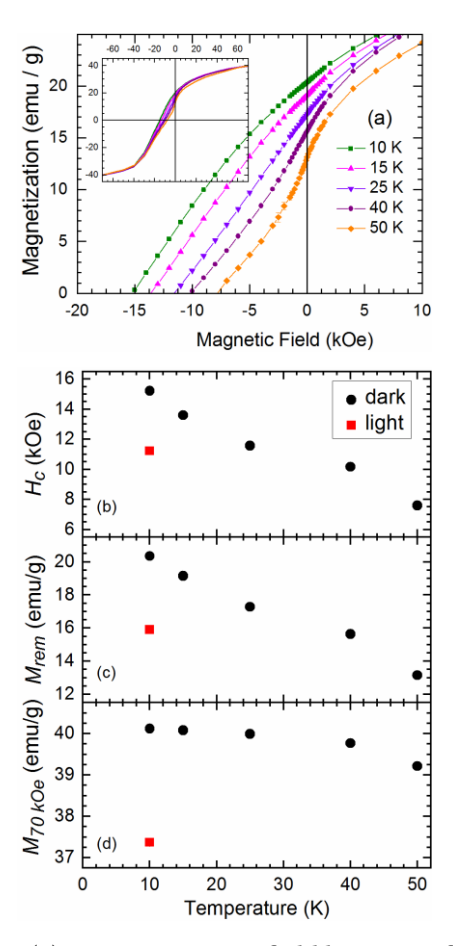


Figure 4. (a) magnetization vs field hysteresis for 3 in the dark at different temperatures. (b-d) Comparisons of the light-activated changes of coercivity, remnant magnetization, and magnetization at 70 kOe for 3 at 10 K to the dark state values of the same sample over the temperature range 10 K – 50 K.

The light-induced decoupling of the exchange coupled magnets can be attributed to the selective demagnetization of the surface spins of the ferrite nanoparticles, as was recently described for single-phase cobalt ferrite and manganese ferrite. For the single phase ferrites, the light-induced decreases in magnetic coercivity and high-field magnetization can be attributed to changes in magnetic volume as irradiation decouples the weakly coupled surface spins of the high surface-to-volume ratio nanoparticles. The likely explanation for the surface selectivity is effective heating of the electronic reservoir near the surface

mediated by skin-depth absorption. At low temperatures the electronic reservoir can be effectively decoupled from the macroscopic lattice limiting the light-induced thermal jump to the surface spins, which experience weaker magnetic coupling than the bulk because of surface disorder and lower number of nearest neighbors. For the previously studied cobalt ferrite, the light-induced effects were larger for aggregates than for nanoparticles isolated by surfactant coatings as the surface spin decoupling also weakened interparticle coupling. In exchange coupled heterostructures selective demagnetization of the surface spins is sufficient to break the exchange coupling while maintaining the bulk magnetization of the two constituents, as observed for compositions 2 and 3.

The present study takes advantage of the concept of using light-induced changes in surface magnetization to design an exchange coupled magnet that can be switched with light. At the same time, the results on the cobalt ferrite/manganese ferrite heterostructures validate the recently proposed explanation for the light-induced demagnetization in ferrite nanoparticles, upon which the current study was based.16 The results provide a new mechanism for designing light-switchable magnetic materials. Using light to decouple exchange coupled magnets is a potential route to decreasing the energy product of a magnetic bit and enabling magnetic recording at lower write head magnetic fields. Since it is only necessary to influence the surface spins, bulk laser heating of the magnetic medium is not required, which could have a great impact on potential applications.

ASSOCIATED CONTENT

Supporting Information. Synthesis and methods, Chemical and particle size analysis, PXRD refinement for **3**. This material is available free of charge via the Internet at http://pubs.acs.org.

AUTHOR INFORMATION

Corresponding Author

* Email: talham@chem.ufl.edu * Email: meisel@phys.ufl.edu

Author Contributions

The manuscript was written through contributions of all authors.

ACKNOWLEDGMENT

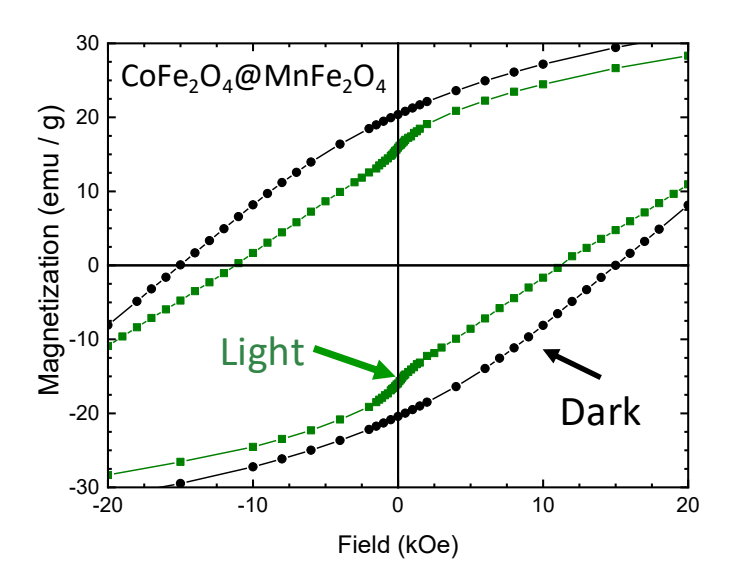
This work was supported in part by the following funding sources: The National Science Foundation via DMR-1405430 and DMR-1904596 (DRT), DMR-1202033 and DMR-1708410 (MWM) and DMR-1157490 and DMR-1644779 (National High Magnetic Field Laboratory); and the University of Florida Division of Sponsored Programs. Use of the Advanced Photon Source at Argonne National Laboratory was supported by the U. S. Department of Energy, Office of Science, Office of Basic Energy Sciences, under Contract No. DE-AC02-06CH11357.

REFERENCES

- 1. Challener, W.; Peng, C.; Itagi, A.; Karns, D.; Peng, W.; Peng, Y.; Yang, X.; Zhu, X.; Gokemeijer, N.; Hsia, Y.; Ju, G.; Rottmayer, R.; Seigler, M.; Gage, E., Heat-assisted magnetic recording by a near-field transducer with efficient optical energy transfer. Nat. Photon. 2009, 3, 220-224.
- 2. McDaniel, T., Areal density limitation in bit-patterned, heat-assisted magnetic recording using FePtX media. J. Appl. Phys. 2012, 112, 093920.
- 3. Elphick, K.; Vallejo-Fernandez, G.; Klemmer, T.; Thiele, J.; O'Grady, K., HAMR media based on exchange bias. Appl. Phys. Lett. 2016, 109, 052402.
- 4. El Hadri, M.; Hehn, M.; Malinowski, G.; Mangin, S., Materials and devices for all-optical helicity-dependent switching. J. Phys D-Appl. Phys 2017, 50, 133002.
- 5. Liu, F.; Hou, Y.; Gao, S., Exchange-coupled nanocomposites: chemical synthesis, characterization and applications. Chem. Soc. Rev. 2014, 43, 8098-8113.
- 6. Bader, S. D. Opportunities in nanomagnetism. Rev. Mod. Phys. 2006, 78, 1-15.
- 7. López-Ortega, A.; Estrader, M.; Salazar-Alvarez, G.; Roca, A. G.; Nogués, J., Applications of exchange coupled bi-magnetic hard/soft and soft/hard magnetic core/shell nanoparticles. Phys. Rep. 2015, 553, 1-32.
- 8. Song, Q.; Zhang, Z. J., Controlled Synthesis and Magnetic Properties of Bimagnetic Spinel Ferrite CoFe₂O₄ and MnFe₂O₄ Nanocrystals with Core-Shell Architecture. J. Am. Chem. Soc. 2012, 134, 10182-10190.
- 9. Rostamnejadi, A.; Venkatesan, M.; Salamati, H.; Ackland, K.; Gholizadeh, H.; Kameli, P.; Coey, J., Magnetic properties, exchange bias, and memory effects in core-shell superparamagnetic nanoparticles of Lao.67Sro.33MnO3. J. Appl. Phys. 2017, 121, 173902.
- 10. Skumryev, V.; Stoyanov, S.; Zhang, Y.; Hadjipanayis, G.; Givord, D.; Nogues, J. Beating the superparamagnetic limit with exchange bias. Nature 2003, 423 (6942), 850.
- 11. Phan, M.; Alonso, J.; Khurshid, H.; Lampen-Kelley, P.; Chandra, S.; Repa, K.; Nemati, Z.; Das, R.; Iglesias, O.; Srikanth, H., Exchange Bias Effects in Iron Oxide-Based Nanoparticle Systems. Nanomat. 2016, 6, 221.
- 12. Liu, J. P. F., E; Gutfleisch, O; Sellmyer, D. J. Nanoscale Magnetic Materials and Applications. 2009, 309.
- Nandwana, V.; Chaubey, G. S.; Yano, K.; Rong, C.-B.; Liu, J. P. Bimagnetic nanoparticles with enhanced exchange coupling and energy products. Journal of Applied Physics 2009, 105 (1), 014303.
- 14. Giri, A. K.; Pellerin, K.; Pongsaksawad, W.; Sorescu, M.; Majetich, S. A., Effect of light on the magnetic properties of cobalt ferrite nanoparticles. IEEE Trans. Mag. 2000, 36, 3029-3031.
- 15. Giri, A. K.; Kirkpatrick, E. M.; Moongkhamklang, P.; Majetich, S. A.; Harris, V. G., Photomagnetism and structure in cobalt ferrite nanoparticles. Appl. Phys. Lett. 2002, 80, 2341-2343.
- 16. Brinzari, T.; Rajan, D.; Ferreira, C.; Stoian, S.; Quintero, P.; Meisel, M.; Talham, D., Light-induced magnetization changes in aggregated and isolated cobalt ferrite nanoparticles. J. Appl. Phys. 2018, 124, 103904.

- 17. Haneda, K.; Morrish, A. H., Noncollinear magnetic-structure of CoFe₂O₄ small particles. J. Appl. Phys. 1988, 63, 4258-4260.
- 18. Kodama, R. H.; Berkowitz, A. E.; McNiff, E. J.; Foner, S., Surface spin disorder in NiFe2O4 nanoparticles. Phys. Rev. Lett. 1996, 77, 394-397.
- 19. Morales, M. P.; Veintemillas-Verdaguer, S.; Montero, M. I.; Serna, C. J.; Roig, A.; Casas, L.; Martinez, B.; Sandiumenge, F., Surface and internal spin canting in gamma-Fe₂O₃ nanoparticles. Chem. Mater. 1999, 11, 3058-3064.
- 20. Krycka, K.; Borchers, J.; Booth, R.; Ijiri, Y.; Hasz, K.; Rhyne, J.; Majetich, S., Origin of Surface Canting within Fe₃O₄ Nanoparticles. Phys. Revs Lett. 2014, 113, 147203.
- 21. Ijiri, Y.; Krycka, K.; Hunt-Isaak, I.; Pan, H.; Hsieh, J.; Borchers, J.; Rhyne, J.; Oberdick, S.; Abdelgawad, A.; Majetich, S., Correlated spin canting in ordered core-shell Fe₃O₄/MnxFe₃-xO₄ nanoparticle assemblies. Phys. Rev. B 2019, 99, 094421.
- 22. Oberdick, S.; Abdelgawad, A.; Moya, C.; Mesbahi-Vasey, S.; Kepaptsoglou, D.; Lazarov, V.; Evans, R.; Meilak, D.; Skoropata, E.; van Lierop, J.; Hunt-Isaak, I.; Pan, H.; Ijiri, Y.; Krycka, K.; Borchers, J.; Majetich, S., Spin canting across core/shell Fe₃O₄/MnFe₃-xO₄ nanoparticles. Sci. Rep. 2018, 8, 3425.
- 23. Zeng, H.; Sun, S.; Li, J.; Wang, Z. L.; Liu, J. P., Tailoring magnetic properties of core/shell nanoparticles. Appl. Phys. Lett. 2004, 85, 792-794.
- 24. Masala, O.; Hoffman, D.; Sundaram, N.; Page, K.; Proffen, T.; Lawes, G.; Seshadri, R., Preparation of magnetic spinel ferrite core/shell nanoparticles: Soft ferrites on hard ferrites and vice versa. Solid State Sci. 2006, 8, 1015-1022.
- 25. Brabers, V. A. M. Progress in spinel ferrite research, in Handbook of Magnetic Materials, Buschow, K. H. J., Ed., Elsevier, 1995, 8, pp. 189 324.
- 26. Skomski, R.; Coey, J. M. D. Giant energy product in nanostructured two-phase magnets. Physical Review B 1993, 48, 15812.
- 27. Xie, Y.; Vincent, A.; Chang, H.; Rinehart, J., Strengthening nanocomposite magnetism through microemulsion synthesis. Nano Research 2018, 11, 4133-4141.
- 28. Pahwa, C.; Mahadevan, S.; Narang, S.; Sharma, P. Structural, magnetic and microwave properties of exchange coupled and non-exchange coupled BaFe12O19/NiFe2O4 nanocomposites. Journal of Alloys and Compounds 2017, 725, 1175.
- 29. Almessiere, M.; Slimani, Y.; Baykal, A., Exchange spring magnetic behavior of Sro.3Bao.4Pbo.3Fe12O19/(CuFe2O4)x nanocomposites fabricated by a one-pot citrate sol-gel combustion method. J. Alloys Compd. 2018, 762, 389-397.
- 30. Hazra, S.; Patra, M.; Vadera, S.; Ghosh, N., A Novel But Simple "One-Pot" Synthetic Route for Preparation of (NiFe₂O₄)x(BaFe₁₂O₁₉)₁-x Composites. J. Am. Cer. Soc. 2012, 95, 60-63.

TOC Graphic:



Supporting Information for

A Light-Switchable Exchange-Coupled Magnet

Divya Rajan, [†] John M. Cain, [†] Tatiana Brinzari, [†] Caue F. Ferreira, [†] Nicholas G. Rudawski, [‡] Ashley C. Felts, [†] Mark W. Meisel, [‡] Daniel R. Talham [†]*

[†]Department of Chemistry, University of Florida, Gainesville, FL 32611-7200, USA

^tDepartment of Physics and National High Magnetic Field Laboratory,

University of Florida, Gainesville, FL 32611-8440, USA

[†] Herbert Wertheim College of Engineering, University of Florida, Gainesville, FL-32611, USA

Corresponding Authors

* Email: talham@chem.ufl.edu * Email: meisel@phys.ufl.edu

Synthesis and Methods

Samples were synthesized using a coprecipitation method as described in the literature. S1

Cobalt ferrite particles, 1, $Co_{0.94}Fe_{2.06}O_4$. Cobalt chloride, $CoCl_2 \cdot 6H_2O$ (5 mmol), and ferric chloride, $FeCl_3 \cdot 6H_2O$ (10 mmol), were dissolved in 50 mL of nanopure water. This solution was added dropwise (using an addition funnel) to a solution prepared by dissolving NaOH (0.15 mol) in 100 mL nanopure water. After complete addition, the mixture was heated at 90° C for 1.5 hours. After cooling to room temperature, the black solution was added to six 50 mL centrifuge tubes and filled with nanopure water up to the 30 mL mark and centrifuged for 10 min @ 9000 rpm. After decanting the supernatant, the remaining reaction mixture was added to the existing centrifuge tubes, and after filling the tubes with water up to the 30 mL mark centrifugation was performed as before. After decanting the supernatant, the black residue from the centrifuge tubes was transferred to one tube and nanopure water was added up to a volume of 45 mL, and this suspension was stored in the refrigerator and treated as the core stock solution. High resolution powder X-ray diffraction pattern of the sample was indexed to a spinel ferrite phase, Fd-3m (JCPDS PDF#221086). ICP data: (Co:Fe) = 1.00: (2.18 \pm 0.03). Particle size is 12 \pm 4 nm within 250 \pm 70 nm aggregates.

Cobalt ferrite/Manganese ferrite core@shell-like particles, 2. Co_{0.94}Fe_{2.06}O₄/Mn_{0.94}Fe_{2.06}O₄.

The seed particle suspension (5 mL) was added to 195 mL of nanopure water in a 1000 mL round bottom flask. An aqueous solution (100 mL) of MnCl₂·6H₂O (0.2 mmol) and FeCl₃·6H₂O (0.4 mmol) and an equal volume of solution containing NaOH (0.03 mol) were simultaneously added dropwise to the core suspension using a peristaltic pump at an addition speed of 10 mL/hour. After complete addition, the reaction mixture was heated at 90° C for 1.5 hours. The black precipitate obtained was washed with nanopure water and acetone and dried under nitrogen. High resolution powder X-ray diffraction pattern of the sample was indexed to two components, each with a spinel ferrite phase, Fd-3m (JCPDS PDF#221086). ICP data: Assuming the Co:Fe ratio within the cobalt ferrite component is unchanged relative to the seed particles, ICP yields (Mn:Fe) =1.00:(2.26 \pm 0.03) and a CoFe₂O₄/ MnFe₂O₄ ratio of 1:1, consistent with the precursor amounts used in the synthesis. Particle size is 16 \pm 4 nm within aggregates of 270 \pm 80 nm.

Cobalt ferrite/Manganese ferrite mixture, 3. Manganese chloride, MnCl₂·6H₂O (1.67 mmol), cobalt chloride, CoCl₂·6H₂O (3.33 mmol), ferric chloride, FeCl₃·6H₂O (10 mmol), were dissolved in 100 mL of nanopure water. This solution was added dropwise (using an addition funnel) to a solution prepared by dissolving NaOH (0.375 mol) in 100 mL nanopure water. After complete addition, the mixture was heated at 90° C for 1.5 hours. The reaction mixture was washed with

nanopure water and acetone to obtain a black powder upon drying under nitrogen. High resolution powder X-ray diffraction pattern of the sample was indexed to two components, each with a spinel ferrite phase, Fd-3m (JCPDS PDF#221086). ICP data: (Mn:Co:Fe) =1.00:(1.91 \pm 0.05): (5.66 \pm 0.15), consistent with a 1:2 manganese ferrite/cobalt ferrite ratio of the precursors. Particle size is 4 \pm 1 nm within aggregates of 250 \pm 70 nm.

Structural Characterization

Inductively coupled plasma atomic emission spectroscopy recorded on a Perkin-Elmer Optima 3200 instrument was used to determine the Co:Fe ratios in the samples. Transmission electron microscopy (TEM) and associated energy dispersive spectroscopy (EDS) was used to study the structure and composition of the particles. A JEOL 2010F operating at 200 kV was used for bright-field TEM (BF-TEM) imaging to assess particle shape. Additionally, a JEOL ARM200cF (Cs-corrected in scanning mode) equipped with a Gatan GIF Quantum SE energy filter was used to perform high-angle annular dark-field scanning TEM (HAADF-STEM) imaging and electron energy loss spectroscopy (EELS) mapping. High resolution powder X-ray diffraction patterns were collected using beamline 11-BM at the Advanced Photon Source (APS, Argonne National Laboratory, Argonne, IL).

Magnetic Characterization

The dc magnetic properties were investigated using a commercial superconducting quantum interference device (SQUID) magnetometer (Quantum Design MPMS-XL7). The optical measurements were performed with a homemade quartz optic sample rod attached to a tungsten halogen lamp via a fiber optic patch cable (400-2200 nm). The power at the sample calibrated outside the squid magnetometer was approximately 4 mW. The samples were prepared by dispersing the cobalt ferrite nanoparticles (1% by weight) in an optical grade epoxy (Stycast 1266). The sample dimensions were approximately 0.12 cm x 0.13 cm (r x h). As an alternative approach, nanoparticles can also be spread as a thin layer between two pieces of transparent tape; however due to the high absorption of cobalt ferrite, the amount of material strongly influences the magnitude of the photomagnetic effect. The dilution of cobalt ferrite is a critical step in the investigation of its photomagnetic properties, so samples mixed with epoxy were used in this work. The magnetization vs. field/temperature dependence in the dark state was measured after field cooling the sample in 0.01 kOe from room temperature. Irradiation experiments at a particular temperature were performed in a field of 0.01 kOe after field cooling the sample from room temperature. After achieving saturation, the magnetization in the light state was measured under constant irradiation.

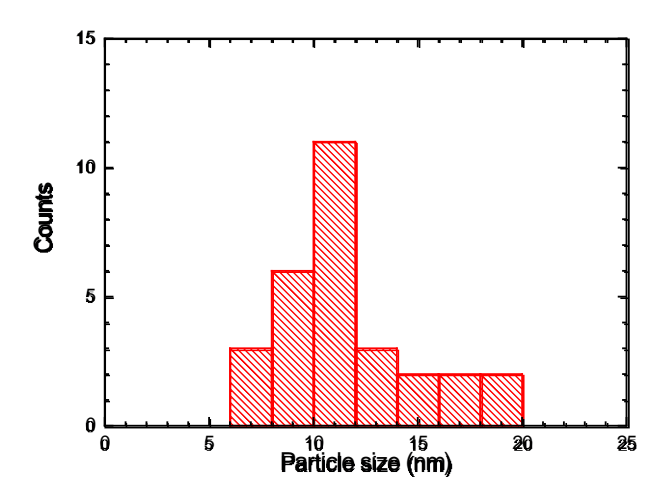


Figure S1. Particle size distribution for $Co_{0.94}Fe_{2.06}O_4$, **1**, corresponding to Figure 1 in the text.

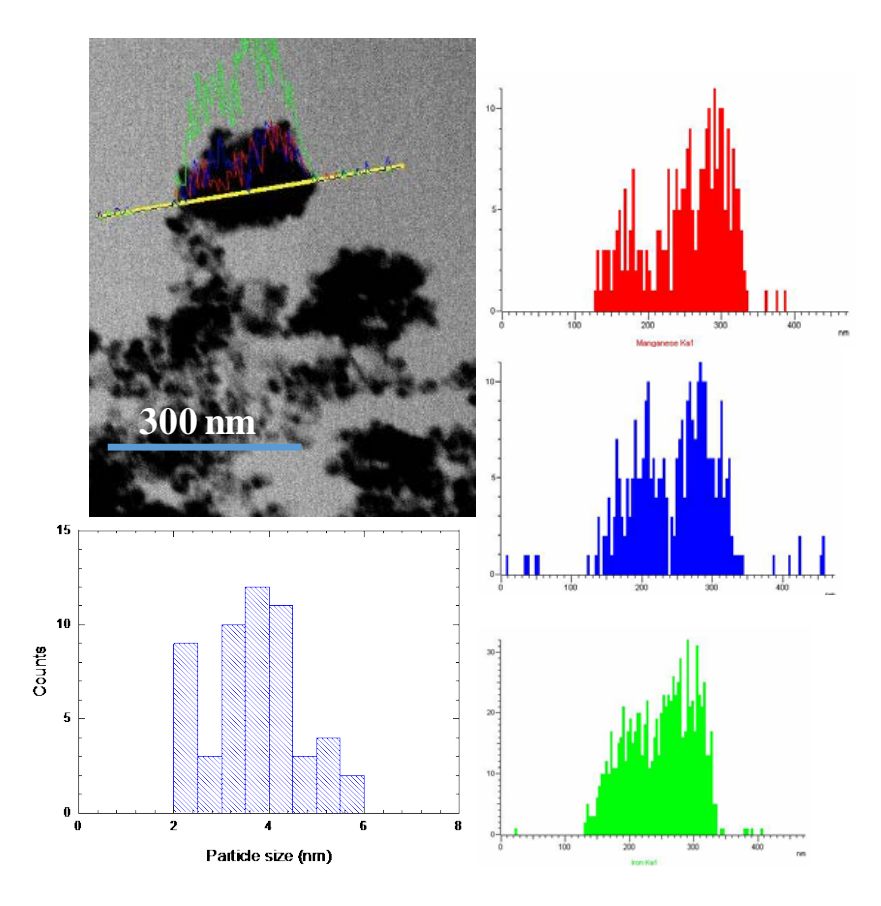
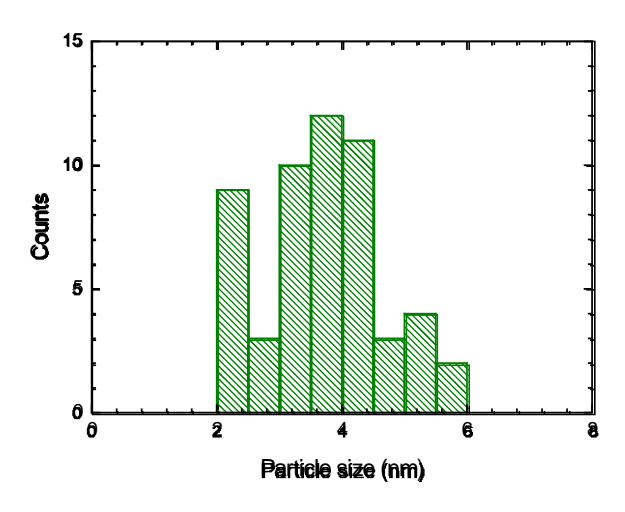


Figure S2. Characterization of cobalt ferrite/manganese ferrite core@shell-like particles, **2.** TEM image with corresponding EDS linescans for manganese (green), cobalt(blue) and iron (red) and particle size histogram.



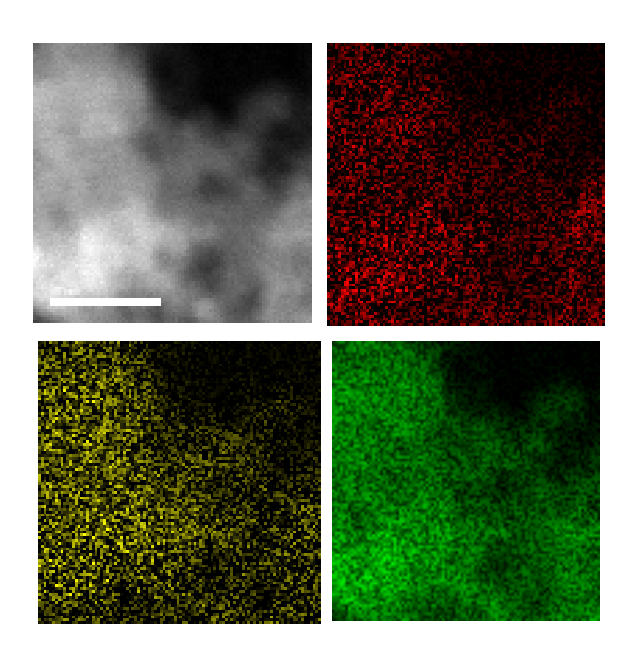


Figure S3. Particle size distribution for **3**, corresponding to Figure 3 in the text. TEM image (scale bar is 10 nm) and corresponding EELS maps for Mn (red), Co (yellow) and Fe (green) within an aggregate of **3**.

PXRD Refinement for 3.

To determine whether **3** is better described as a heterogeneous composite of as a solid solution Rietveld analysis was performed on PXRD data collected at the APS. The Rietveld method¹ is generally a powerful technique for determining the macroscopic and microscopic properties of polycrystalline materials. In this case, though, due to the small difference in the scattering strengths of manganese, iron, and cobalt, a good fit to the two-phase model is insufficient evidence without simultaneous, independent rejection of the alternative, a single-phase solid solution model. Here, Pawley ('structure-free') refinements were performed first to determine the best possible profile fit and the values of the non-structural parameters, followed by Rietveld refinement to elucidate the sample composition.² Fitting was performed first considering sample 3 as a two-phase mixture, then the fitting was restarted, this time considering sample 3 to be a single-phase solid solution. The quality of the fit and the chemical plausibility of the results were then used as evidence to support the presence of two chemically distinct phases.

Rietveld refinements proceeded using a structural model determined through analysis of the Co^{II} $2p_{3/2}$ and Fe^{III} $2p_{3/2}$ peaks and the parameters obtained from the Pawley fits.³ Fitting was performed using GSAS-II (v. 3788).⁴ Restraints were needed to damp the rate of composition change during the refinement; these restraints had an initially high weight (10^6) which was slowly reduced to a very small value (0.01). The background, crystallite sizes, microstrain (if applicable), and lattice parameters were refined periodically during this process, and all were refined simultaneously at the end of the refinement. The obtained compositions and sample parameters are listed in Table 2. U_{iso} was set to 0.01 for all atoms and was not refined, as this variable has a strong correlation with site occupancy.² Fourier difference maps were generated for each phase at the end of the refinement which each show a maximum electron density difference of less than $1 e/A^3$.

The results of the Rietveld refinements are compared graphically in Figure S4, and the parameters characterizing each fit are provided in Table S1. In general, the two-phase model provides a more satisfactory fit to the observed data than the solid solution model. Additionally, in order to produce a moderately commensurate fit using the solid solution model, background peaks needed to be introduced which were not observed in the empty capillary pattern,⁵ and peak broadening corrections due to anisotropic microstrain were necessary.⁶ These corrections have a questionable physical basis in our sample which lends further support to the two-phase model as the better representation.

The phase compositions from the two Rietveld refinements, and other sample parameters, are listed in Tables S2 and S3. For the fit using the single-phase solid solution model, despite starting the refinement with a 1:1.91 Mn:Co ratio, the best agreement with the data is a

model which contains only cobalt and iron. The composition of this cobalt ferrite phase is consistent (within error) with that of the cobalt ferrite phase obtained in the two-phase Rietveld refinement. In the two-phase refinement, the manganese ferrite is present as a series of broad peaks at the base of the much sharper cobalt ferrite peaks, and these broad lines are absorbed into the background in the solid-solution refinements. It is clear the solid solution model yields a poor fit to the data and can be rejected as a candidate.

Focusing now on the two-phase refinement, by comparing the phase fractions and site occupancies for each element to the elemental ratios obtained from ICP-AES, it is estimated that only approximately 70% of the cobalt in the sample is accounted for by the cobalt ferrite. The remainder may contribute to the broad peaks assigned to the manganese ferrite, providing a possible explanation for the relatively small manganese ferrite lattice parameter compared to single-phase manganese ferrite (a = 8.50 Å). The lattice parameter for the cobalt ferrite is also shifted with respect to the single-phase sample (a = 8.35 Å), however, this change is in good agreement with the expected increase due to the higher cobalt fraction relative to the single-phase sample.^{7,8} Finally, a summation of the nominal charges on each ion over all of the sites in the unit cell yields a result which seems to violate charge neutrality, however, the chargeneutral composition is within the combined error of the composition determinations.

In summary, through the application of the Rietveld method to synchrotron powder X-ray diffraction data, the two-phase model has been shown to provide a satisfactory fit, while the alternative, a single-phase solid solution model fits the data poorly, yielding physically unrealistic sample parameters, and is therefore rejected.

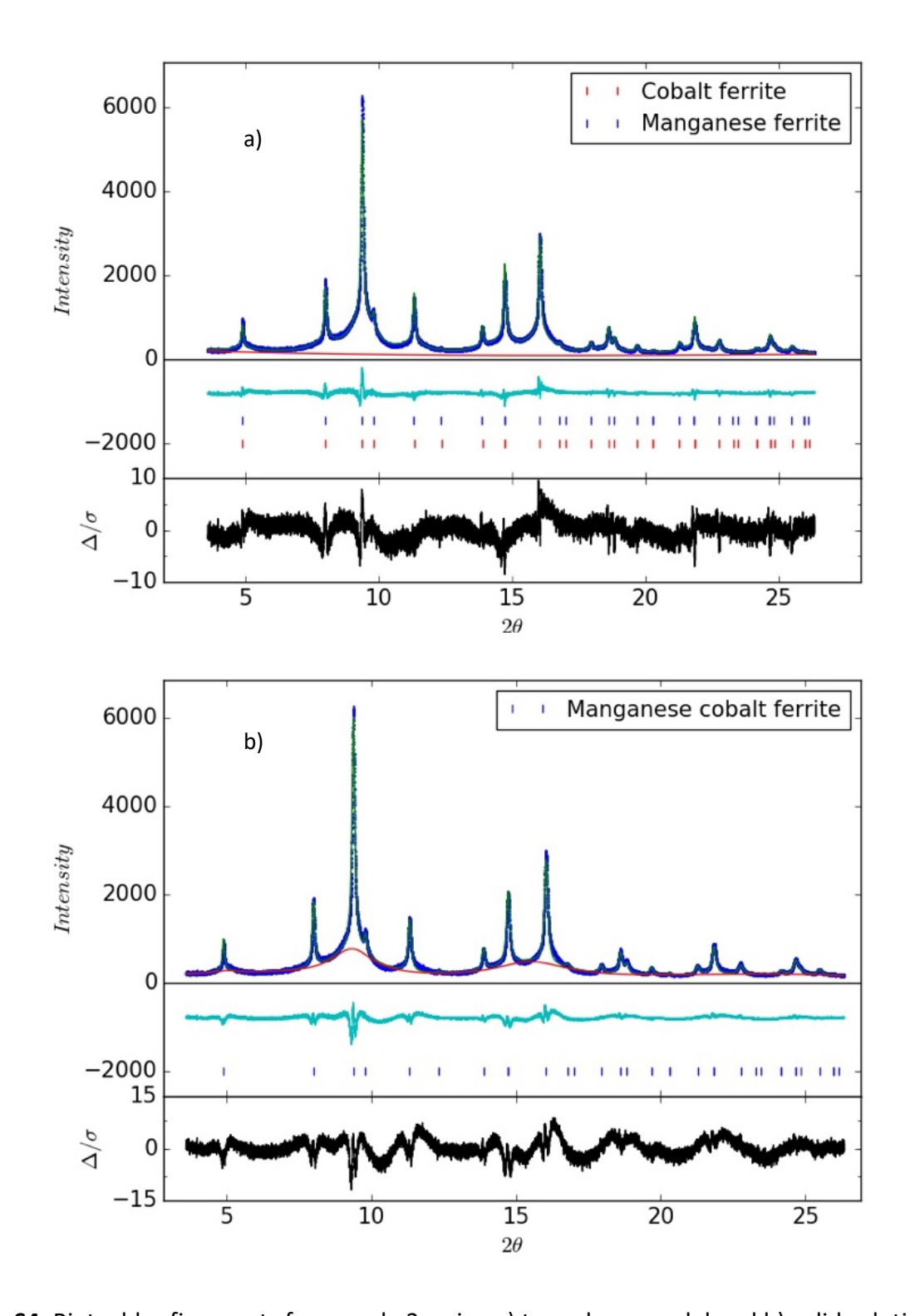


Figure S4. Rietveld refinements for sample 3, using a) two-phase model and b) solid solution model.

Table S1. Fit statistics for Rietveld refinements using two-phase and solid solution models.

Model	R _{wp}	χ ²	R _F , cobalt ferrite	R _F , manganese ferrite	R _F , cobalt manganese ferrite
Two-phase	7.72%	1.78	2.05%	1.43%	-
Solid solution	10.20%	2.38	-	-	6.65%

Table S2. Refined parameters for two-phase model.

Phase	а	Crystallite size	Composition	Phase fraction
Cobalt ferrite	8.39 Å	26 nm	(Co _{0.4} Fe _{0.5})[Co _{0.48} Fe _{0.54}] ₂ O _{4.0}	27.4%
Manganese ferrite	8.40 Å	3 nm	(Mn _{0.3} Fe _{0.6})[Mn _{0.3} Fe _{0.6}] ₂ O ₄	72.6%

Table S3. Refined parameters for solid solution model.

Composition	а	Crystallite size	S ₄₀₀	S ₂₂₀
(Mn _{0.0} Co _{0.5} Fe _{0.4})[Mn _{0.0} Co _{0.5} Fe _{0.5}] ₂ O _{4.0}	8.40 Å	31 nm	0.0172	0.0016

References, Supporting Information:

- (S1) Tang, Z. M.; Sorensen, C. M.; Klabunde, K, J. and Hadjipanayis. G. C. "Size-dependent Curie temperature in nanoscale MnFe₂O₄ particles" *Phys. Rev. Lett.* **1991**, *67*, 3602-3605.
- (S2) Rietveld, H. "A profile refinement method for nuclear and magnetic structures" *J. Appl. Cryst.* **1969**, *2*, 65-71.
- (S3) McCusker, L. B.; Von Dreele, R. B.; Cox, D. E.; Louër, D.; Scardi, P. "Rietveld refinement guidelines" *J. Appl. Cryst.* **1999**, *32*, 36-50.
- (S4) Zhou, Z.; Zhang, Y.; Wang, Z.; Wei, W.; Tang, W.; Shi, J.; Xiong, R. "Electronic structure studies of the spinel CoFe₂O₄ by X-ray photoelectron spectroscopy." *Appl. Surf. Sci.* **2008**, *254*, 6972–6975.
- (S5) Toby, B. H.; Von Dreele, R. B. "GSAS-II: "The genesis of a modern open-source all purpose crystallography sortware package" *J. Appl. Cryst.* **2013**, *46*, 544-549.
- (S6) "Empty 11-BM Kapton sample capillary," https://wikiext.aps.anl.gov/ug11bm/index.php/Standards Data (accessed Mar 20, 2019).

- (S7) Stephens, P. W. "Phenomenological model of anisotropic peak broadening in powder diffraction" *J. Appl. Cryst.* **1999**, *32*, 281–289.
- (S8) Bhongale, G. M.; Kulkarni, D. K.; Sapre, V. B. "New formula for lattice dimension of an oxide spinel with cubic structure" *Bull. Mater. Sci.* **1992**, *15*, 121–125.
- (S9) Shannon, R. D. "Revised effective ionic radii and systematic studies of interatomic distances in halides and chalcogenides" *Acta Cryst.* **1976**, *A32*, 751-767.